Comparison of Satellite and Geomorphic Indices for Flooded Areas Detection in a Mediterranean River Basin

Vincenzo Totaro(✉), Giuseppe Peschechera, Andrea Gioia, Vito Iacobellis, and Umberto Fratino

Politecnico di Bari, Via Orabona 4, Bari 70125, Italy
{vincenzo.totaro, giuseppe.peschechera, andrea.gioia, vito.iacobellis, umberto.fratino}@poliba.it

Abstract. Flood-hazard map delineation is an important task in planning land management activities. This evaluation is usually based on coupled hydraulic/hydrological models, which often require time consuming and expensive measurement campaigns in order to estimate the necessary distributed physical information for their implementation (e.g. digital elevation models, land cover and geological maps); moreover, the observed effects of flood events are needed for their calibration and validation. The obtained flooded maps can allow to perform geomorphic DEM-based procedure, which is a valid tool useful for the rapid identification and mapping of flood-prone areas; in addition remote sensing is a reliable and widespread source of input data for the application of hydrological and hydraulic models: particular interest generate the attitude of the Landsat-8 OLISR data in the definition of the effective flooded area. The goal of this work is to compare performances of remote sensing and DEM-based techniques for the definition of flood-prone areas, using as reference map that obtained by a two-dimensional hydraulic simulation. An objective comparison between these two approaches has been carried out(using linear binary classifiers method and ROC curves) on the case study of Lato river basin, located in the Puglia region, Southern Italy; the satellite indices showed good performances even if the selected geomorphic descriptors still remain the most performing in reproducing the inundated areas.

Keywords: Geomorphological descriptors · Flooded areas · Satellite indices · Hydraulic model

1 Introduction

Natural disasters, such as floods and droughts, have devastating social, environmental and economic implications for many areas of the world. With the aim to reduce and mitigate the effects of such phenomena, in the latest few years flood-hazard map delineation is assuming a growing interest.

© Springer Nature Switzerland AG 2019
S. Misra et al. (Eds.): ICCSA 2019, LNCS 11622, pp. 173–185, 2019.
https://doi.org/10.1007/978-3-030-24305-0_14

The evaluation of floodable areas is usually carried out by applying coupled hydrological and hydraulic models: the former are used for the definition of a flood event (e.g. [1–10]), the latter are exploited for performing flood propagation (e.g. [11–16]); this approach, in more cases, involves lot of human and informatic resources for its parametrization; moreover it needs time consuming and expensive measurement campaigns for the estimation of the required inputs distributed information and observed data useful for calibration and validation.

In order to satisfy the increasing requirements of end users (like Basin Authorities, Civil Protection agencies) and the needs of recent legislation on flood risk protection (e.g. Floods Directive 2007/60/EC), a necessary upgrade of theoretical approaches used for mapping the hydraulic hazard level of the territory is needed with the purpose to mitigate and contain the catastrophic effects of the inundations, which are becoming more frequent in recent decades. Moreover, the increasing availability of high-resolution topographical data (i.e. digital terrain models - DTMs) due to new technologies for the measurement of surface elevation (i.e. Light Detection And Ranging - LiDAR) gives strong impulse to the increasing development of new DTM-based techniques (e.g. [17, 18]) able to provide a rapid and reliable identification of flood susceptibility maps (e.g. [19–21]) using only geomorphological information, in areas characterized by poor hydrological information..

Recently, in addition to these consolidated methodologies, the evolution of surface phenomena can be monitored also using remote sensing techniques [22–33], providing good performances in investigating indices [21, 34] useful for the rapid identification of inundated areas.

Interesting developments of such methodologies can be conducted considering multiple case studies on a wide area for the evaluation at regional scale (e.g. [35]) or extending the proposed approach to other fields of application (e.g. [36, 37]).

In this study satellite and geomorphic indices for flooded areas detection are compared on the Lato river basin located in Puglia Region (southern Italy), in order to evaluate their reliability in representing reference maps of inundated area, estimated using a classical approach of a combined hydrological and hydraulic model.

2 Case Study

The proposed analysis is focused on the Lato river which, flowing into the Gulf of Taranto (Ionian Sea), receives the runoff contributions of Castellaneta and Laterza municipalities, located in the Taranto province (Fig. 1). His length is about 5 km and his basin area has an extension of about 670 km^2. The analysis was performed on a flood event that occurred downstream of the Lato river in the days of 6/7 October 2013.

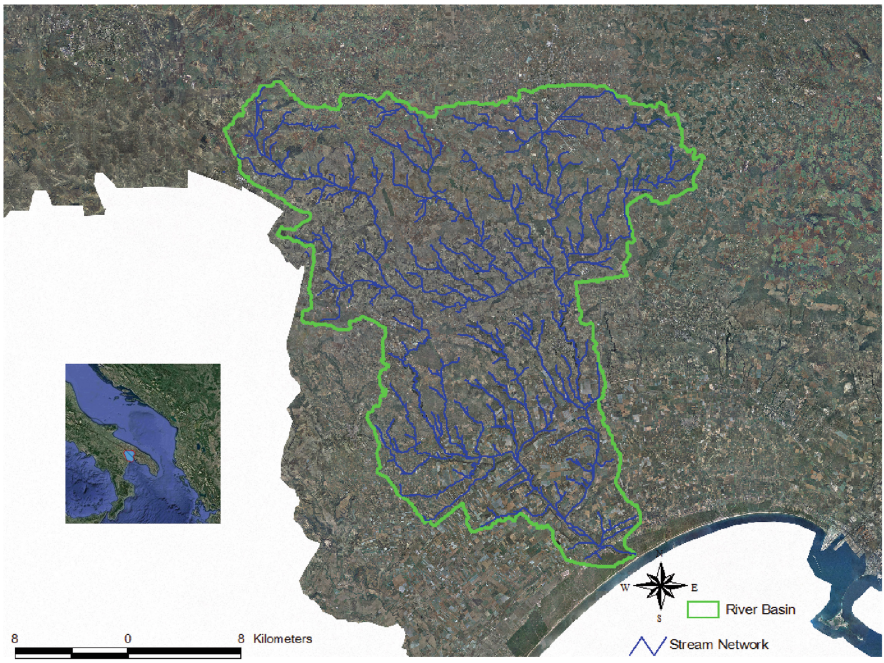

Fig. 1. Study area. Coordinate System UTM WGS 84 zone 33 N.

3 Methodologies

In this section the following topics are illustrated:

- the definition of flooded area (used as reference map) by exploiting hydrologic/hydraulic models;
- flood-prone areas evaluation, using satellite and geomorphic descriptors;
- the selection of the most appropriate basin descriptor through binary classifiers and Receiver Operating Characteristic method.

3.1 Hydrologic/Hydraulic Modeling

Flooded area generated by the investigated meteorological event has been delineated by coupling a two-dimensional hydraulic model (FLO 2D [38]) with the CN-SCS hydrological model (USDA-SCA [39]) for the estimation of the flood hydrograph. In particular the numerical simulation was conducted over the computational grid within the selected Digital Terrain Model and the flood event was reproduced introducing the simulated hydrograph as boundary condition. The hydraulic modeling has been calibrated using flooded areas (with return periods of 30 and 200 years) extracted from the database of the Basin Authority of Puglia for the investigated study area (e.g. http://www.adb.puglia.it/public/news.php).

3.2 Satellite Basin Descriptors

In this study a single post flooding Landsat 8 Operational Land Imager (OLI) acquired on 10th October 2013 (LC08188032201310100 1T) was used. The Landsat 8 mission was developed inherited the properties of the previous Landsat products in terms of spatial, spectral, and temporal (16 days) resolutions. The sensor OLI consists of eight spectral bands (bands 1–7 and 9) with a moderate spatial resolution of 30 meters, and a panchromatic band (Pan) with a higher resolution (15 m). Despite the moderate spatial resolution of the sensor, it is provided of one band in the Near Infrared (NIR) and two in the Short Wave Infrared (SWIR) which are useful for analysing water surfaces and plant water content [32, 40]. The image used in the present work was downloaded radiometrically, geometrically and atmospherically corrected (Level-2, on-demand) from the USGS website. The Landsat-8 Surface Reflectance data (L8SR) are generated using the radiative transfer model Landsat 8 Surface Reflectance Code (LaSRC), a novel algorithm that performs better than the previous (Landsat Ecosystem Disturbance Adaptive Processing System) due to the use of the coastal aerosol band and of auxiliary climate data from MODIS [41].

The OLISR image was used for the identification of the flooded area following the band-ratio approach and testing different SR indices dedicated to water surfaces mapping retrieved in literature. Moreover, as shows by other Authors, due to the difficulties in mapping water surfaces under canopy vegetation, which limit water surface, three vegetation indices were also tested [42]. All these indices exploit the information from the visible and the infrared (both NIR and SWIR) regions. The list of the adopted indices is provided in Table 1.

The Simple Ratio (SR) is the simplest ratio-based vegetation index based on the ratio between the reflectance recorded in the NIR and Red bands usually used to distinguish green leaves from other objects in the scene for example, soil and water [43]. The Normalized Difference Vegetation Index (NDVI) is one of the widely index used for measure of healthy, green vegetation [44]. It is obtained as normalized difference between the NIR and red reflectance and therefore results functionally, but not linearly, equivalent to the SR. The NDVI has a finite validity range (from –1 to +1) while the SR is always positive with an infinite range (0 to infinity), which can be a practical disadvantage as compared to NDVI. However, is demonstrated that also the NDVI tends to saturate for dense vegetation. For optimizing the vegetation signal in areas of high leaf area index, was developed the Enhanced vegetation index (EVI). Moreover, due to the use of the blue reflectance region, it corrects the soil background signals and reduces atmospheric influences [45]. All these vegetation indices are usually used for vegetation monitoring and classification, while in this work were used for mapping floods.

The Normalized Difference Water Index (NDWI) was introduced by McFeeters to enhance water features maximizing its reflectance in the visible domain (by using green wavelengths) and minimizing the reflectance of NIR [46]. However, due to the similar reflectance pattern of built-up land and water in the green band, water features extracted include false positives from built-up land, which overestimates the area of extracted water. Hence a modified NDWI (MNDWI) was developed, in which the SWIR band was used to replace the NIR band in the NDWI in order to enhance open water features

(which are characterized by higher absorption in the SWIR region than in NIR) while efficiently suppressing, and even removing, built-up land, vegetation and soil noise. For this reason, it is more suitable for enhancing and extracting water features in contexts dominated by built-up land areas [47]. Another modification of the NDWI was used in the present study, the Land Surface Water Index (LSWI). It uses the NIR and the SWIR regions of the electromagnetic spectrum and, thanks to the strong light absorption by liquid water in the SWIR, it is sensitive to the total amount of liquid water in vegetation and its soil background. It is worth to mention that the index has different nomenclatures: Gao [48] called it NDWI while Wilson et al. called it Normalized Difference Moisture Index (NDMI) [49].

Lastly, we tested the Automated Water Extraction Index (AWEI). The AWEI was developed to improve water extraction accuracy in the presence of various sorts of environmental noise that other classification methods often fail to classify correctly (including shadow and dark surfaces) and at the same time offers a stable threshold value [50].

Table 1. List of multispectral indices used for the identification of the flooded area.

Index	References
$SR = \frac{\rho_{NIR}}{\rho_{Red}}$	[43]
$\text{NDVI} = \frac{\rho_{red} - \rho_{NIR}}{\rho_{red} + \rho_{NIR}}$	[51]
$EVI = 2.5 \times \frac{\rho_{NIR} - \rho_{Red}}{\rho_{NIR} + 6\rho_{Red} - 7.5\rho_{Blue} + 0.5}$	[45]
$\text{NDWI} = \frac{\rho_{green} - \rho_{NIR}}{\rho_{green} + \rho_{NIR}}$	[46]
$\text{MNDWI}^* = \frac{\rho_{green} - \rho_{SWIR}}{\rho_{green} + \rho_{SWIR}}$	[47]
$\text{AWEI} = 4 \times (\rho_{Green} - \rho_{SWIR1}) - (0.25\rho_{NIR} + 2.75\rho_{SWIR2})$	[50]

*Two indices calculated for respectively SWIR-1and SWIR-2

3.3 Morphological Basin Descriptors

Geomorphic indices are useful tools for evaluating flood-prone areas in a very fast way; they can reflect the behaviors of inundated areas. In this context previous evaluation have been already carried out on the same investigated case study (e.g. [21]); in this paper an integration analysis including the application of the Receiver Operating Characteristic (ROC) approach is introduced. For sake of brevity only the best performant indices are explained, but the reader can find a complete description in [21]:

- *elevation to the nearest stream, H [m]:* this index computes the elevation difference between a considered cell on the river basin and that hydrologically connected on the stream network.
- $ln(h_r/H)$ (Gemomorphic Flood Index, GFI): this index relates, for each point on the river basin, the water depth h_r with the synthetic descriptor H, where h_r can be defined as:

$$h_r \cong bA_r^n \tag{1}$$

with A_r [m^2] upslope contributing area calculated at the hydrologically connected point on the stream network, b a scale factor usually set equal to 10^{-2} and n a dimensionless exponent set equal to 0.3.

3.4 Linear Binary Classifiers and ROC Curves Methods

The methodology for performing calibration of indices, using linear binary classifiers and ROC methods, has been explained by a step-by-step procedure in [52]. It requires to scale and normalize the descriptor maps considering values ranging between –1 and 1. Then, applying a moving threshold with an assigned step (10^{-3} in this case), binary (0–1) maps are obtained. Using this approach, each cell on the investigated domain may be classified as True Positive (TP), False Positive (FP), True Negative (TN) and False Negative (FN), by a comparison with reference binary map. In order to define the threshold with the lowest rate of errors, the following Objective Function (OB) is computed for each selected threshold:

$$OB = r_{fp} + \left(1 - r_{tp}\right) \tag{2}$$

where r_{fp} and r_{tp} are:

$$r_{tp} = \frac{TP}{TP + FN} \tag{3}$$

$$r_{fp} = \frac{FP}{FP + TN} \tag{4}$$

The best index is that with the lowest value of the objective function, while flooded maps can be obtained applying the corresponding normalized threshold τ_{norm} to the index map.

The ROC approach [53] is a useful tool for testing the performances of the investigated indices, relating r_{tp} and r_{fp}. The measure of the goodness of fit, for each considered index, is obtained calculating the Area Under Curve (AUC) on the selected investigated domain.

4 Results and Discussion

The application of linear binary classifier and ROC tests has been conducted on satellite indices described in the Sect. 3.2, leading to the results shown in Table 2 and Fig. 2.

The minimum values of the objective function range between 0.375 and 0.401, showing similar performances. A more detailed analysis can be performed looking at the true positive (r_{tp}) and false positive rate (r_{fp}), defined as in (3) and (4) respectively and reported in Table 2, and observing the related calibrated flooded maps, reported in Fig. 3. Reference flooded map is reported in the top left of the Fig. 3.

Table 2. Results of the linear binary classifier test and Area Under Curve evaluation for the investigated satellite descriptors.

	τ_{norm}	r_{fp}	r_{tp}	*min*(OB)	AUC
SR	–0.883	0.088	0.713	0.375	0.895
NDVI	0.153	0.089	0.714	0.375	0.895
EVI	0.144	0.079	0.700	0.378	0.894
NDWI	–0.333	0.107	0.736	0.371	0.898
MNDWI SWIR 1	–0.451	0.096	0.748	0.348	0.878
MNDWI SWIR 2	–0.022	0.070	0.676	0.394	0.865
AWEI	0.350	0.026	0.625	0.401	0.836

Following the criterion of choosing the index characterized by the lowest value of the objective function, the best performant index is the MNDWI SWIR 1, but it can be interesting to carry out a more detailed analysis. In fact, the AWEI index has the lowest rate of false positive, as it can be confirmed by looking at the Fig. 3: the AWEI flooded map has really a small percentage of inundated cells outside the real flooded area, revealing an interesting performance in the false positive detection. However, this advantage disappears if we look at the true positive rate, which assumes the lowest value respect to the other descriptors. In this case, the best ability in recognizing inundated cells is performed by the MNDWI SWIR 1 index.

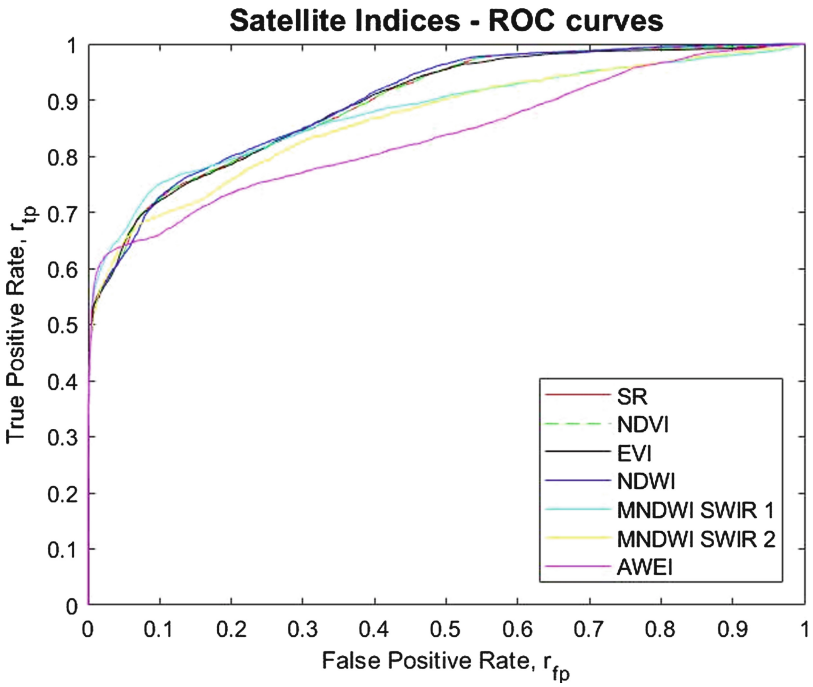

Fig. 2. ROC curves for satellite indices

The best compromise between the true positive (r_{tp}) and false positive rate (r_{fp}) is achieved by minimizing the objective function.

Similitudes between satellite indices shown in Table 2 can also be observed looking at the Fig. 2, where the Receiver Operating Characteristic curves are shown. In fact, the curves are pretty similar, and the AWEI is the index with lowest performance, whose curve reflects, moreover, its ability in detecting the false positive.

Figure 3 shows the comparison between the flooded area reference map (on the top left) retrieved by using the hydraulic modelling and those estimated using the surface reflectance indices. All the indices are not suitable to retrieve the mainstream, due to

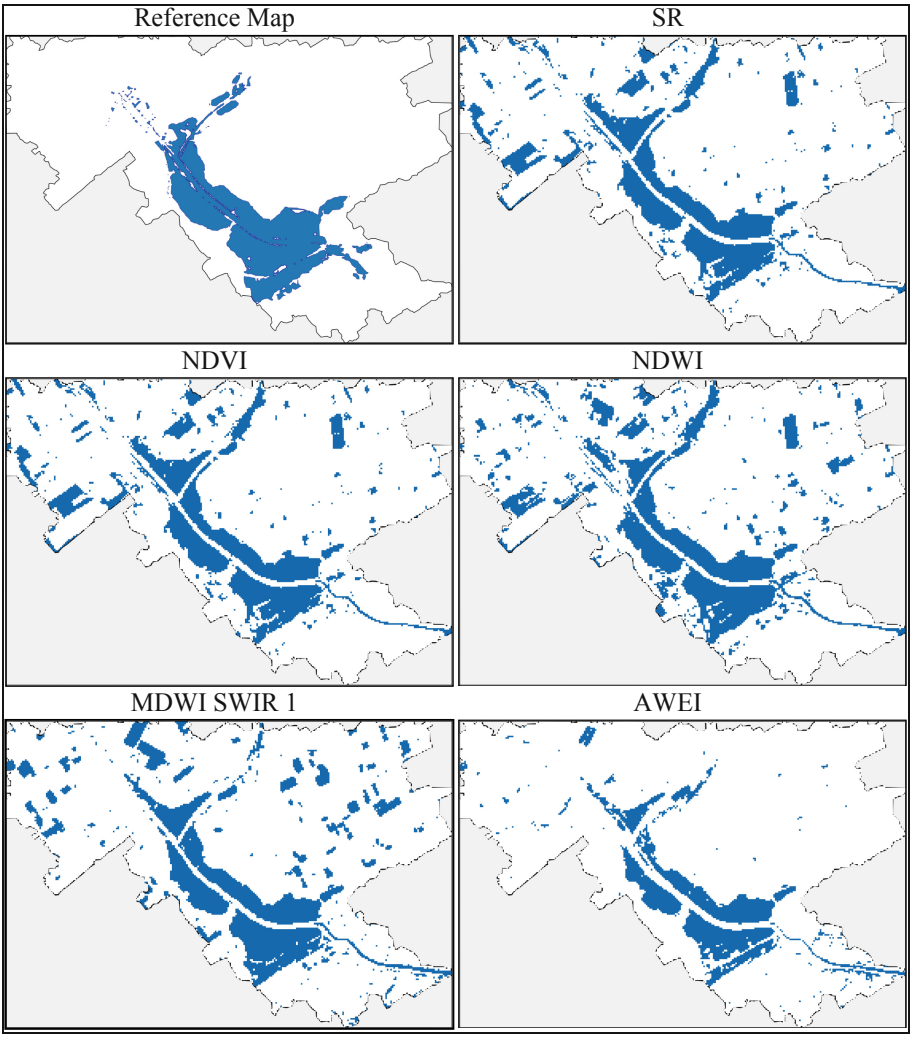

Fig. 3. Comparisonbetween the reference map and flooded areas obtained through calibration procedure applied to some satellite descriptors.

the presence of the riparian vegetation. The vegetation indices (SR, NDVI, EVI), based on Red and NIR bands, can reproduce the same area, with an overestimation of false flooded areas. Only the AWEI index reduces the cases of false flooding estimation, even if it underestimates the extension of the true flooded area.

Results of the linear binary classifiers test for the geomorphic indices H and GFI, indicated as the most performants in a previous research(21), are already reported in this study. In particular, looking at the ROC curves showed in Fig. 4, it is possible to observe similar performances for the selected indices, whose AUC and OB values are reported in Table 3. Moreover, it is quite evident how geomorphic descriptors are suitable to reproduce floodable areas really better than satellite indices, avoiding false positive values far from the real flood-prone zone. More in detail, while false positive rate is low for both indices, it is very important to note the ability of the H descriptor in detecting true positive cells. In particular, their physical link with the river network is a strong element for justifying its excellent performances.

Table 3. Results of linear binary classifier test and Area Under Curve evaluation for the selected geomorphic descriptors

	τ_{norm}	r_{fp}	r_{tp}	*min*(OB)	AUC
H	–0.975	0.051	0.941	0.110	0.981
GFI	–0.231	0.057	0.746	0.211	0.970

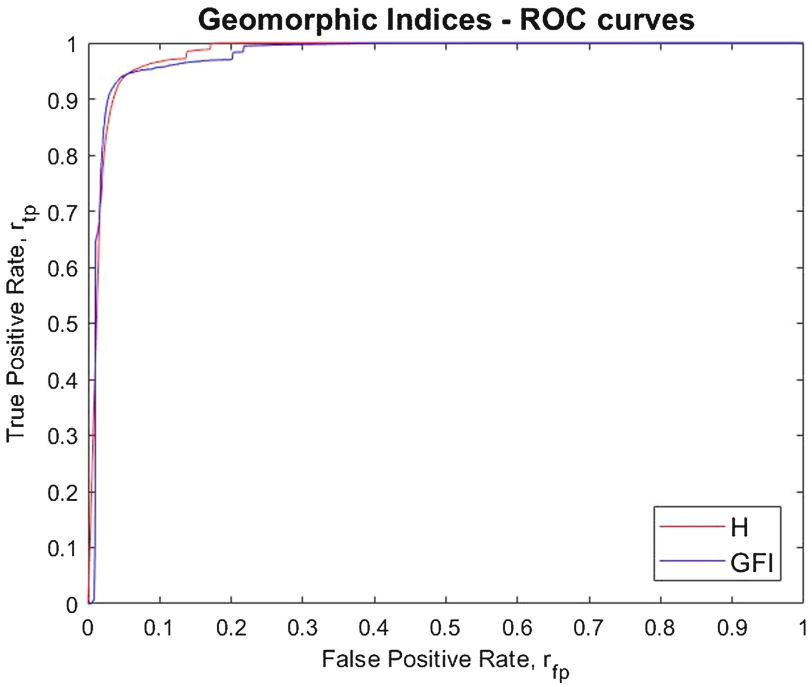

Fig. 4. ROC curves for geomorphic indices

5 Conclusions

In this paper an investigation on the ability of satellite indices in detecting flood-prone areas has been carried out. Despite the lag-time between the observed flood event and the first available satellite image (about three days), the results of the linear binary classifiers approach and Receiver Operating Characteristic curves methodology are very promising; in particular the existing lag-time may influence the capacity in detecting true positive flooded areas. Notwithstanding the good performances showed by the satellite indices on the investigated study area, the selected geomorphic descriptors (H and GFI) still remain the most performing in reproducing the inundated areas. The increasing availability of satellite products can help the scientific community in the development of new techniques for a rapid flood-prone areas identification. However, further investigations on the possibility of using these images should be conducted, for an aware knowledge in the context of hydraulic applications.

References

1. Feldman, A.D.: Hydrologic modeling system HEC-HMS. Technical reference manual (2000)
2. Fiorentino, M., Gioia, A., Iacobellis, V., Manfreda, S.: Analysis on flood generation processes by means of a continuous simulation model. In: Advances in Geosciences, pp. 231–236. Copernicus GmbH (2006). https://doi.org/10.5194/adgeo-7-231-2006
3. Beven, K.J.: Rainfall-Runoff Modelling: The Primer, 2nd edn. (2012)
4. Manfreda, S.: Performance of a Theoretical Model for the Description of Water Balance and Runoff Dynamics in Southern Italy (2014)
5. Gorgoglione, A., Gioia, A., Iacobellis, V., Piccinni, A.F., Ranieri, E.: A rationale for pollutograph evaluation in ungauged areas, using daily rainfall patterns: case studies of the Apulian region in Southern Italy. Appl. Environ. Soil Sci. **2016**, 1–16 (2016). https://doi.org/10.1155/2016/9327614
6. Gioia, A., Iacobellis, V., Manfreda, S., Fiorentino, M.: Comparison of different methods describing the peak runoff contributing areas during floods. Hydrol. Process. **31**, 2041–2049 (2017). https://doi.org/10.1002/hyp.11169
7. Gioia, A.: Reservoir routing on double-peak design flood. Water **8**, 553 (2016). https://doi.org/10.3390/w8120553
8. Gioia, A., Iacobellis, V., Manfreda, S., Fiorentino, M.: Influence of infiltration and soil storage capacity on the skewness of the annual maximum flood peaks in a theoretically derived distribution. Hydrol. Earth Syst. Sci. **16**, 937–951 (2012). https://doi.org/10.5194/hess-16-937-2012
9. Iacobellis, V., Fiorentino, M., Gioia, A., Manfreda, S.: Best fit and selection of theoretical flood frequency distributions based on different runoff generation mechanisms. Water **2**, 239–256 (2010). https://doi.org/10.3390/w2020239
10. Iacobellis, V., et al.: Investigation of a flood event occurred on Lama Balice, in the context of hazard map evaluation in karstic-ephemeral streams. In: Gervasi, O., et al. (eds.) ICCSA 2018. LNCS, vol. 10964, pp. 317–333. Springer, Cham (2018). https://doi.org/10.1007/978-3-319-95174-4_26
11. De Wrachien, D., Mambretti, S.: Mathematical models for flood hazard assessment. Int. J. SAFE. **1**, 353–362 (2011). https://doi.org/10.2495/SAFE-V1-N4-353-362

12. Iacobellis, V., Castorani, A., Di Santo, A.R., Gioia, A.: Rationale for flood prediction in karst endorheic areas. J. Arid Environ. **112**, 98–108 (2015). https://doi.org/10.1016/j.jaridenv.2014.05.018
13. Bates, P.D., Anderson, M.G., Price, D.A., Hardy, R.J., Smith, C.N.: Analysis and development of hydraulic models for floodplain flow. In: Floodplain Processes, pp. 215–254 (1996)
14. Jain, S.K., Singh, R.D., Jain, M.K., Lohani, A.K.: Delineation of flood-prone areas using remote sensing techniques. Water Resour. Manage **19**, 333–347 (2005). https://doi.org/10.1007/s11269-005-3281-5
15. Fluet-Chouinard, E., Lehner, B., Rebelo, L.-M., Papa, F., Hamilton, S.K.: Development of a global inundation map at high spatial resolution from topographic downscaling of coarse-scale remote sensing data. Remote Sens. Environ. **158**, 348–361 (2015). https://doi.org/10.1016/j.rse.2014.10.015
16. Manfreda, S., et al.: Flood-prone areas assessment using linear binary classifiers based on flood maps obtained from 1D and 2D hydraulic models. Nat. Hazards J. Int. Soc. Prev. Mitig. Nat. Hazards **79**, 735–754 (2015)
17. Nardi, F., Vivoni, E., Grimaldi, S.: Investigating a floodplain scaling relation using a hydrogeomorphic delineation method. Water Resour. Res. **42** (2006). https://doi.org/10.1029/2005WR004155
18. Marks, K., Bates, P.: Integration of high-resolution topographic data with floodplain flow models. Hydrol. Process. **14**, 2109–2122 (2000)
19. Degiorgis, M., Gnecco, G., Gorni, S., Roth, G., Sanguineti, M., Taramasso, A.C.: Classifiers for the detection of flood-prone areas using remote sensed elevation data. J. Hydrol. **470–471**, 302–315 (2012). https://doi.org/10.1016/j.jhydrol.2012.09.006
20. De Risi, R., Jalayer, F., De Paola, F., Giugni, M.: Probabilistic delineation of flood-prone areas based on a digital elevation model and the extent of historical flooding: the case of Ouagadougou. Bol. Geol. Min. **125**, 329–340 (2014)
21. Totaro, V., Gioia, A., Novelli, A., Caradonna, G.: The use of geomorphological descriptors and landsat-8 spectral indices data for flood areas evaluation: a case study of Lato river basin. In: Gervasi, O., et al. (eds.) ICCSA 2017. LNCS, vol. 10407, pp. 30–44. Springer, Cham (2017). https://doi.org/10.1007/978-3-319-62401-3_3
22. Mattia, F., et al.: Time series of COSMO-SkyMed data for landcover classification and surface parameter retrieval over agricultural sites. In: 2012 IEEE International Geoscience and Remote Sensing Symposium, pp. 6511–6514 (2012). https://doi.org/10.1109/IGARSS.2012.6352738
23. Balenzano, A., et al.: On the use of multi-temporal series of COSMO-SkyMed data for LANDcover classification and surface parameter retrieval over agricultural sites. In: 2011 IEEE International Geoscience and Remote Sensing Symposium, pp. 142–145 (2011). https://doi.org/10.1109/IGARSS.2011.6048918
24. Balenzano, A., et al.: A ground network for SAR-derived soil moisture product calibration, validation and exploitation in Southern Italy. In: 2014 IEEE Geoscience and Remote Sensing Symposium, pp. 3382–3385 (2014). https://doi.org/10.1109/IGARSS.2014.6947206
25. Olang, L.O., Kundu, P., Bauer, T., Fürst, J.: Analysis of spatio-temporal land cover changes for hydrological impact assessment within the Nyando River Basin of Kenya. Environ. Monit. Assess. **179**, 389–401 (2011). https://doi.org/10.1007/s10661-010-1743-6
26. Balacco, G., Figorito, B., Tarantino, E., Gioia, A., Iacobellis, V.: Space–time LAI variability in Northern Puglia (Italy) from SPOT VGT data. Environ. Monit. Assess. **187**, 434 (2015). https://doi.org/10.1007/s10661-015-4603-6
27. Crocetto, N., Tarantino, E.: A class-oriented Strategy for features extraction from multidate ASTER imagery. Remote Sens. **1**, 1171–1189 (2009). https://doi.org/10.3390/rs1041171

28. Saradjian, M.R., Hosseini, M.: Soil moisture estimation by using multipolarization SAR image. Adv. Space Res. **48**, 278–286 (2011). https://doi.org/10.1016/j.asr.2011.03.029
29. Iacobellis, V., Gioia, A., Milella, P., Satalino, G., Balenzano, A., Mattia, F.: Inter-comparison of hydrological model simulations with time series of SAR-derived soil moisture maps. Euro. J. Remote Sens. **46**, 739–757 (2013). https://doi.org/10.5721/EuJRS20134644
30. Tarantino, E.: Monitoring spatial and temporal distribution of sea surface temperature with TIR sensor data. Ital. J. Remote Sens. **44**(1), 97–107 (2012)
31. Aquilino, M., Novelli, A., Tarantino, E., Iacobellis, V., Gentile, F.: Evaluating the potential of GeoEye data in retrieving LAI at watershed scale. In: Presented at the Remote Sensing of the Ocean, Sea Ice, Coastal Waters, and Large Water Regions 1 October 2014 (2014). https://doi.org/10.1117/12.2067185
32. Peschechera, G., Novelli, A., Caradonna, G., Fratino, U.: Calibration of the CLAIR model by using landsat 8 surface reflectance higher-level data and MODIS leaf area index products. In: Gervasi, O., et al. (eds.) ICCSA 2017. LNCS, vol. 10407, pp. 16–29. Springer, Cham (2017). https://doi.org/10.1007/978-3-319-62401-3_2
33. Peschechera, G., Fratino, U.: Calibration of CLAIR model by means of Sentinel-2 LAI data for analysing wheat crops through landsat-8 surface reflectance data. In: Gervasi, O., et al. (eds.) ICCSA 2018. LNCS, vol. 10964, pp. 294–304. Springer, Cham (2018). https://doi.org/10.1007/978-3-319-95174-4_24
34. Gioia, A., Totaro, V., Bonelli, R., Esposito, A.A.M.G., Balacco, G., Iacobellis, V.: Flood susceptibility evaluation on ephemeral streams of Southern Italy: a case study of Lama Balice. In: Gervasi, O., et al. (eds.) ICCSA 2018. LNCS, vol. 10964, pp. 334–348. Springer, Cham (2018). https://doi.org/10.1007/978-3-319-95174-4_27
35. Fiorentino, M., Gioia, A., Iacobellis, V., Manfreda, S.: Regional analysis of runoff thresholds behaviour in Southern Italy based on theoretically derived distributions. In: Advances in Geosciences, pp. 139–144. Copernicus GmbH (2011). https://doi.org/10.5194/adgeo-26-139-2011
36. Valentino, S., Costa, P.J., Humberto, V., Giuseppina, U., Fabio, F.: Structural degradation assessment of RC buildings: calibration and comparison of semeiotic-based methodology for decision support system. J. Perform. Constructed Facil. **33**, 04018109 (2019). https://doi.org/10.1061/(ASCE)CF.1943-5509.0001249
37. Valentino, S., Giuseppina, U., Fabio, F.: User reporting-based semeiotic assessment of existing building stock at the regional scale. J. Perform. Constructed Facil. **32**, 04018079 (2018). https://doi.org/10.1061/(ASCE)CF.1943-5509.0001227
38. O'Brien, J.S., Julien, P.Y., Fullerton, W.T.: Two-dimensional water flood and mudflow simulation. J. Hydraul. Eng. **119**, 244–261 (1993). https://doi.org/10.1061/(ASCE)0733-9429(1993)119:2(244)
39. Service, U.S.S.C.: SCS National Engineering Handbook, Section 4: Hydrology (1972)
40. Chen, D., Huang, J., Jackson, T.J.: Vegetation water content estimation for corn and soybeans using spectral indices derived from MODIS near- and short-wave infrared bands. Remote Sens. Environ. **98**, 225–236 (2005). https://doi.org/10.1016/j.rse.2005.07.008
41. Vermote, E., Justice, C., Claverie, M., Franch, B.: Preliminary analysis of the performance of the Landsat 8/OLI land surface reflectance product. Remote Sens. Environ. **185**, 46–56 (2016). https://doi.org/10.1016/j.rse.2016.04.008
42. Malinowski, R., Groom, G., Schwanghart, W., Heckrath, G.: Detection and delineation of localized flooding from WorldView-2 multispectral data. Remote Sens. **7**, 14853–14875 (2015). https://doi.org/10.3390/rs71114853
43. Birth, G.S., McVey, G.R.: Measuring the color of growing turf with a reflectance spectrophotometer 1. Agron. J. **60**, 640–643 (1968). https://doi.org/10.2134/agronj1968.00021962006000060016x

44. Rouse, J.W.: Monitoring vegetation systems in the Great Plains with ERTS. Presented at the 1 January (1974)
45. Huete, A., Didan, K., Miura, T., Rodriguez, E.P., Gao, X., Ferreira, L.G.: Overview of the radiometric and biophysical performance of the MODIS vegetation indices. Remote Sens. Environ. **83**, 195–213 (2002). https://doi.org/10.1016/S0034-4257(02)00096-2
46. McFeeters, S.K.: The use of the normalized difference water index (NDWI) in the delineation of open water features. Int. J. Remote Sens. **17**, 1425–1432 (1996). https://doi.org/10.1080/01431169608948714
47. Xu, H.: Modification of normalised difference water index (NDWI) to enhance open water features in remotely sensed imagery. Int. J. Remote Sens. **27**, 3025–3033 (2006). https://doi.org/10.1080/01431160600589179
48. Gao, B.: NDWI—a normalized difference water index for remote sensing of vegetation liquid water from space. Remote Sens. Environ. **58**, 257–266 (1996). https://doi.org/10.1016/S0034-4257(96)00067-3
49. Wilson, E.H., Sader, S.A.: Detection of forest harvest type using multiple dates of Landsat TM imagery. Remote Sens. Environ. **80**, 385–396 (2002). https://doi.org/10.1016/S0034-4257(01)00318-2
50. Feyisa, G.L., Meilby, H., Fensholt, R., Proud, S.R.: Automated water extraction index: a new technique for surface water mapping using Landsat imagery. Remote Sens. Environ. **140**, 23–35 (2014). https://doi.org/10.1016/j.rse.2013.08.029
51. Rouse Jr., J.W., Haas, R.H., Schell, J.A., Deering, D.W.: Monitoring Vegetation Systems in the Great Plains with Erts, vol. 351, pp. 309. NASA Special Publication (1974)
52. Balacco, G., Totaro, V., Gioia, A., Piccinni, A.F.: Evaluation of geomorphic descriptors thresholds for flood prone areas detection on ephemeral streams in the metropolitan area of Bari (Italy). In: Misra, S., et al. (eds.) ICCSA 2019. LNCS, vol. 11622, pp. 239–254. Springer, Cham (2019)
53. Fawcett, T.: An introduction to ROC analysis. Pattern Recogn. Lett. **27**, 861–874 (2006). https://doi.org/10.1016/j.patrec.2005.10.010